AAPT PHYSICS EDUCATION | AMERICAN JOURNAL of PHYSICS

The use of the stationary phase method as a mathematical tool to determine the path of optical beams

Silvânia A. Carvalho and Stefano De Leo

Citation: American Journal of Physics **83**, 249 (2015); doi: 10.1119/1.4898044
View online: http://dx.doi.org/10.1119/1.4898044
View Table of Contents: http://scitation.aip.org/content/aapt/journal/ajp/83/3?ver=pdfcov
Published by the American Association of Physics Teachers

The use of the stationary phase method as a mathematical tool to determine the path of optical beams

Silvânia A. Carvalho and Stefano De Leo[a)]
Department of Applied Mathematics, State University of Campinas, 13083-859 Brazil

(Received 30 July 2013; accepted 1 October 2014)

We use the stationary phase method to determine the paths of optical beams that propagate through a dielectric block. In the presence of partial internal reflection, we recover the geometrical result obtained by using Snell's law. For total internal reflection, the stationary phase method overreaches Snell's law, predicting the Goos-Hänchen shift. © *2015 American Association of Physics Teachers.*
[http://dx.doi.org/10.1119/1.4898044]

I. INTRODUCTION

Optical beams propagating through dielectrics with dimensions greater than the wavelength of light can be described by rays obeying a set of geometrical rules.[1–3] In this limit, Snell's law is used to determine the relationship between the incidence and refraction angles and, consequently, the paths of optical beams.[4–9] In this paper, we discuss beam propagation through the dielectric block illustrated in Fig. 1, and, as the first step in our analysis (Sec. II), we calculate its geometrical path using Snell's law.

The analogy between optics[1,2] and quantum mechanics[10,11] has been a matter of discussion in recent works.[12,13] The possibility of linking Maxwell's equations for photon propagation in the presence of dielectric blocks with the quantum-mechanical equations for the propagation of electrons in the presence of potential steps[14–16] allows one to determine, in a simple and intuitive way, the reflection and transmission coefficients at the dielectric block interfaces.[17–20] As the second step in our analysis (Sec. III), we obtain the reflection and transmission coefficients for *s*-polarized waves transmitted through the dielectric system of Fig. 1.

Once we obtain the transmission coefficient at the exit interface, we use the stationary phase method (SPM) to calculate the optical path by imposing the cancellation (in the oscillatory electric field integral) of sinusoids with rapidly varying phase.[21–23] The calculation of the position of the maximum of the outgoing beam at the exit of the dielectric block, based on the SPM (Sec. IV), represents an alternative way to obtain the optical path (one that does not require a geometrical analysis). The SPM analysis only requires that we cancel the derivative of the outgoing beam phase. However, the use of the SPM as a mathematical tool to obtain the path of optical beams propagating into dielectric blocks is not simply a matter of taste. For total internal reflection[24,25] the SPM also predicts the Goos-Hänchen (GH) shift,[26–29] demonstrating the importance of the SPM not only to recover Snell's law but also to obtain a typical quantum-mechanical effect. The SPM, illustrated in this paper for calculating the path of optical beams, is a mathematical tool easily extended to other fields of physics in which wave packets play an important role.

Finally, after discussing our conclusions, we extend our results to *p*-polarized waves, suggest how to amplify the GH shift by building a band of dielectric blocks and propose further theoretical investigations.

II. THE OPTICAL PATH VIA SNELL'S LAW

Let us consider an incoming Gaussian beam with waist size w_0 and wavenumber k that moves along the z-direction:[1,2]

$$E_{\rm in}(\mathbf{r}) = E_0\, e^{ikz}\frac{w_0^2}{w_0^2+2iz/k}\exp\left(-\frac{x^2+y^2}{w_0^2+2iz/k}\right), \tag{1}$$

where

$$\mathbf{r} = x\,\mathbf{e}_x + y\,\mathbf{e}_y + z\,\mathbf{e}_z. \tag{2}$$

The plane of incidence is chosen to be the yz-plane. The normals to the left/right and up/down sides of the dielectric block are respectively oriented along the directions of the unit vectors $\mathbf{e}_{\tilde z}$ and $\mathbf{e}_{z_*}$, as shown in Fig. 1. The unit vector $\mathbf{e}_{\tilde z}$ forms an angle θ with $\mathbf{e}_z$, which specifies the direction of the incoming light ray, so that

$$\mathbf{e}_{\tilde y} = \mathbf{e}_y\cos\theta + \mathbf{e}_z\sin\theta, \tag{3}$$

$$\mathbf{e}_{\tilde z} = -\mathbf{e}_y\sin\theta + \mathbf{e}_z\cos\theta. \tag{4}$$

In addition, as can be seen in Fig. 1, $\mathbf{e}_{z_*}$ forms an angle $\pi/4$ with $\mathbf{e}_{\tilde z}$, giving

$$\mathbf{e}_{y_*} = \frac{1}{\sqrt{2}}(\mathbf{e}_{\tilde y} + \mathbf{e}_{\tilde z}), \tag{5}$$

$$d = b\,\cos\theta - c\,\sin\theta + \frac{(b+c)\,\sin 2\theta}{2\sqrt{n^2-\sin^2\theta}}$$

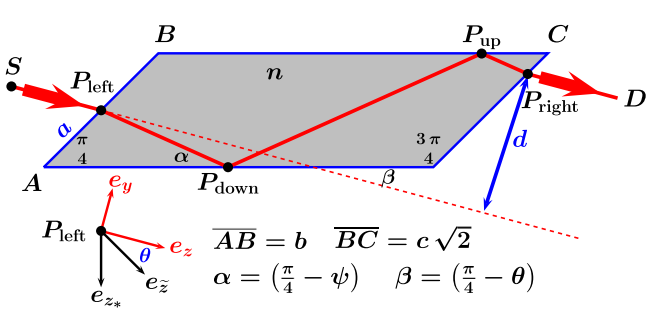

Fig. 1. Geometric layout of the dielectric block used to determine the optical path by Snell's law. The $\tilde z$ and z_* axes represent the normals to the left/right and up/down interfaces, respectively. The origin is chosen at the point where the incoming beam touches the first interface ($P_{\rm left}$). The $\tilde z$-axis is obtained from the z-axis by a clockwise rotation of angle θ.

$$\mathbf{e}_{z_*} = \frac{1}{\sqrt{2}}(-\mathbf{e}_{\tilde{y}} + \mathbf{e}_{\tilde{z}}). \tag{6}$$

In the new coordinates systems, the components of the position vector $\mathbf{r}$ are then related by

$$\begin{aligned}\begin{pmatrix} y_* \\ z_* \end{pmatrix} &= \frac{1}{\sqrt{2}}\begin{pmatrix} 1 & 1 \\ -1 & 1 \end{pmatrix}\begin{pmatrix} \tilde{y} \\ \tilde{z} \end{pmatrix} \\ &= \frac{1}{\sqrt{2}}\begin{pmatrix} 1 & 1 \\ -1 & 1 \end{pmatrix}\begin{pmatrix} \cos\theta & \sin\theta \\ -\sin\theta & \cos\theta \end{pmatrix}\begin{pmatrix} y \\ z \end{pmatrix} \\ &= \mathbf{R}\left(\frac{\pi}{4}+\theta\right)\begin{pmatrix} y \\ z \end{pmatrix},\end{aligned} \tag{7}$$

where $\mathbf{R}$ represents the two-dimensional rotation matrix (note that $x = \tilde{x} = x_*$). The $\{\mathbf{e}_{\tilde{y}}, \mathbf{e}_{\tilde{z}}\}$ and $\{\mathbf{e}_{y_*}, \mathbf{e}_{z_*}\}$ coordinate systems will be used to calculate the geometrical path using Snell's law and to determine the reflection and transmission coefficients of the optical beam.

In order to determine the optical path using Snell's law, we first demonstrate that the outgoing beam is *parallel* to the incoming beam. After that, we calculate the exit point P_{right}, which gives the distance d between the incoming and outgoing beams (see Fig. 1).

When an optical beam falls onto a boundary between two homogeneous media with different refractive indices, it is split into two beams. The refracted (transmitted) beam propagates into the second medium and the reflected beam propagates back into the first medium. For the left air/dielectric boundary in Fig. 1, Snell's law gives

$$\sin\theta = n\sin\psi\,, \tag{8}$$

where n is the index of refraction for the dielectric material, and θ and ψ are the angles that the incident and refracted beams form with the normal $\mathbf{e}_{\tilde{z}}$. In this case, the second medium is optically denser than the first so the refracted angle is a real quantity for all incident angles. The beam propagates into the dielectric block, forming an angle ψ with the $\tilde{z}$-axis and an angle $\pi/4+\psi$ with the z_*-axis. Because the dielectric forms a parallelogram, triangles $AP_{\text{left}}P_{\text{down}}$ and $CP_{\text{right}}P_{\text{up}}$ are similar, so that

$$\angle AP_{\text{down}}P_{\text{left}} = \angle CP_{\text{up}}P_{\text{right}} = \frac{\pi}{4} - \psi \equiv \alpha. \tag{9}$$

Consequently, the optical beam forms an angle ψ with the normal to the right side of the dielectric block (i.e., with $\mathbf{e}_{\tilde{z}}$). Thus, by Snell's law we find that the outgoing beam forms an angle θ with $\mathbf{e}_{\tilde{z}}$, making it parallel to the incoming beam.

We next determine the coordinates of the point P_{right}, where the outgoing beam leaves the block. To do so, it is convenient to use the $\{\mathbf{e}_{y_*}, \mathbf{e}_{z_*}\}$ coordinate system. Without loss of generality, we choose as origin of the coordinate system the incident point on the left (air/dielectric) interface: $\mathbf{P}_{\text{left}} = \{0,0\}$. Using simple geometrical considerations, we find that

$$\begin{aligned}\mathbf{P}_{\text{down}} &= \overline{AP}_{\text{left}}\,\sin\frac{\pi}{4}\left\{\frac{1}{\tan\alpha}, 1\right\} \\ &= \frac{a}{\sqrt{2}}\left\{\tan\left(\frac{\pi}{4}+\psi\right), 1\right\},\end{aligned} \tag{10}$$

where a is the length of segment $\overline{AP}_{\text{left}}$. Similarly, we find that

$$\begin{aligned}\mathbf{P}_{\text{up}} &= \mathbf{P}_{\text{down}} + \overline{AB}\,\sin\frac{\pi}{4}\left\{\frac{1}{\tan\alpha}, -1\right\} \\ &= \frac{1}{\sqrt{2}}\left\{(a+b)\tan\left(\frac{\pi}{4}+\psi\right), (a-b)\right\},\end{aligned} \tag{11}$$

where b is the length of segment $\overline{AB}$. To obtain the coordinates of P_{right} we need to calculate the intersection between the straight line connecting P_{up} and P_{right} ($L1$) and the straight line connecting P_{right} and C ($L2$).

In the $\{\mathbf{e}_{y_*}, \mathbf{e}_{z_*}\}$ system, these straight lines are represented by

$$L1:\ z_* - \frac{a-b}{\sqrt{2}} = \tan\left(\frac{\pi}{4}-\psi\right) \times\left[y_* - \frac{b+a}{\sqrt{2}}\tan\left(\frac{\pi}{4}+\psi\right)\right], \tag{12}$$

$$L2:\ z_* - \frac{a-b}{\sqrt{2}} = -\left[y_* - \left(\frac{b-a}{\sqrt{2}} + c\sqrt{2}\right)\right], \tag{13}$$

where $c\sqrt{2}$ is the length of segment $\overline{BC}$. After simple algebraic manipulations, these equations can be simplified to

$$L1:\ z_* = \tan\left(\frac{\pi}{4}-\psi\right)y_* - b\sqrt{2}, \tag{14}$$

$$L2:\ z_* = -y_* + c\sqrt{2}. \tag{15}$$

Finally, the coordinates for P_{right} can be determined by solving the system (14) and (15), giving

$$\mathbf{P}_{\text{right}} = \left\{\frac{(b+c)\sqrt{2}}{1+\tan\left(\frac{\pi}{4}-\psi\right)}, \frac{\left[c\tan\left(\frac{\pi}{4}-\psi\right)-b\right]\sqrt{2}}{1+\tan\left(\frac{\pi}{4}-\psi\right)}\right\}. \tag{16}$$

Now, given that the path of the incident beam of light is given by the line

$$z_* = y_*\tan\left(\frac{\pi}{4}-\theta\right), \tag{17}$$

we can immediately calculate the (perpendicular) distance between this line and point $\mathbf{P}_{\text{right}}$ as

$$\begin{aligned}d &= \frac{y_*(P_{\text{right}})\tan(\pi/4-\theta) - z_*(P_{\text{right}})}{\sqrt{1+\tan^2(\pi/4-\theta)}} \\ &= \left[b + (b+c)\,\frac{\sin\theta}{\sqrt{n^2-\sin^2\theta}}\right]\cos\theta - c\,\sin\theta\,.\end{aligned} \tag{18}$$

Before concluding this section we note that, depending on the incidence angle θ, the internal reflections can be partial or total. Let us discuss this briefly by calculating the critical angle that characterizes the distinction between partial and total reflection. As discussed earlier, at the first air/dielectric interface the second medium ($n>1$) is optically denser than the first ($n=1$) and we always find a refracted beam that moves into the dielectric block forming a real angle $\psi = \arcsin(\sin\theta/n)$ with the $\tilde{z}$-axis. At the second interface (at P_{down}) we have total internal reflection when

$$n \sin\left(\frac{\pi}{4}+\psi\right) > 1. \tag{19}$$

It is important to note here that for $\psi > \pi/4$ the refracted beam cannot reach the second interface; this represents an additional constraint to be considered in our discussion. By adding this constraint to Eq. (19), we obtain the condition for total internal reflection:

$$\arcsin\left(\frac{1}{n}\right) - \frac{\pi}{4} < \psi < \frac{\pi}{4}. \tag{20}$$

In terms of the incidence angle θ, the previous condition becomes

$$\arcsin\left(\frac{1-\sqrt{n^2-1}}{\sqrt{2}}\right) < \theta < \arcsin\left(\frac{n}{\sqrt{2}}\right). \tag{21}$$

In Fig. 2, we plot the critical angle

$$\theta_c = \arcsin\left(\frac{1-\sqrt{n^2-1}}{\sqrt{2}}\right) \tag{22}$$

as a function of the refractive index n. This curve separates the partial and total reflection zones. We conclude this section by observing that for

$$\frac{1-\sqrt{n^2-1}}{\sqrt{2}} \le -1, \tag{23}$$

which implies

$$n \ge \sqrt{4+2\sqrt{2}}, \tag{24}$$

we *always* find total internal reflection.

III. MAXWELL'S EQUATIONS AND TRANSMISSION COEFFICIENTS

In this section, we calculate the transmission and reflection coefficient at each interface using Maxwell's equations.[1,2] The phase of the outgoing beam will be then used to calculate the path of the optical beam using the stationary phase method[21–23]

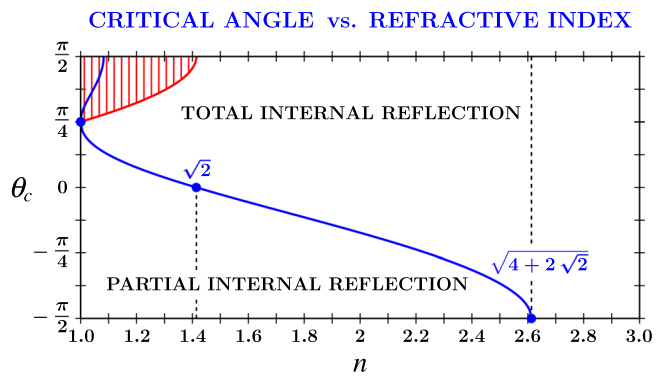

Fig. 2. The critical angle θ_c is plotted as a function of the refractive index n. The forbidden region (shaded) represents incidence angles for which the refracted beam at the left interface cannot reach the down boundary. For $n > \sqrt{4+2\sqrt{2}}$, we always find total internal reflection.

The plane wave solution of

$$\left[\partial_{xx} + \partial_{yy} + \partial_{zz} - \frac{\partial_{tt}}{c^2}\right] E(\mathbf{r},t) = 0 \tag{25}$$

is given by

$$\exp\left[i(k_x x + k_y y + k_z z - \omega t)\right], \tag{26}$$

providing that $k = \sqrt{k_x^2 + k_y^2 + k_z^2} = \omega/c$. Given the linearity of Eq. (25), a superposition of these plane wave solutions will also be a solution. Many lasers emit beams that approximate a Gaussian profile,[18,19,30] given by

$$E(\mathbf{r},t) = E_0 \frac{w_0^2}{4\pi} \int \mathrm{d}k_x\, \mathrm{d}k_y \exp\left[-\left(k_x^2+k_y^2\right)w_0^2/4\right] \times \exp[i(\mathbf{k}\cdot\mathbf{r} - \omega t)], \tag{27}$$

where w_0 is the waist size of the beam. Observe that for $\sqrt{k_x^2+k_y^2} \ll k$ (which constitutes the *paraxial* approximation), the previous integral can be calculated analytically and leads to Eq. (1).

Given that the transmitted (refracted) beam is along the $\tilde{z}$-axis, it is convenient to rewrite Maxwell's equations by using the coordinate system $(x, \tilde{y}, \tilde{z})$:

$$\left[\partial_{xx} + \partial_{\tilde{y}\tilde{y}} + \partial_{\tilde{z}\tilde{z}} - n^2(\tilde{z})\,\frac{\partial_{tt}}{c^2}\right] E_{\text{left}}(\mathbf{r},t) = 0 \tag{28}$$

with

$$n(\tilde{z}) = \begin{cases} 1 & \text{for } \tilde{z} < 0 \\ n & \text{for } \tilde{z} > 0. \end{cases} \tag{29}$$

The plane wave solution is now given by

$$\exp\left[i(k_x x + k_{\tilde{y}}\tilde{y} - \omega t)\right] \times \begin{cases} \exp\left[ik_{\tilde{z}}\tilde{z}\right] + R_{\text{left}} \exp\left[-ik_{\tilde{z}}\tilde{z}\right] & \text{for } \tilde{z} < 0 \\ T_{\text{left}} \exp\left[iq_{\tilde{z}}\tilde{z}\right] & \text{for } \tilde{z} > 0, \end{cases} \tag{30}$$

where

$$\begin{pmatrix} k_{\tilde{y}} \\ k_{\tilde{z}} \end{pmatrix} = \mathbf{R}(\theta) \begin{pmatrix} k_y \\ k_z \end{pmatrix} \tag{31}$$

and

$$\{q_{\tilde{y}}, q_{\tilde{z}}\} = \left\{k_{\tilde{y}}, \sqrt{n^2k^2 - k_x^2 - k_{\tilde{y}}^2}\right\}. \tag{32}$$

Observe that the $\tilde{y}$-component of the wave number does not change because the discontinuity is along the $\tilde{z}$-axis.[31] Imposing the continuity of E_{left} and $\partial_{\tilde{z}} E_{\text{left}}$ at the point where the refractive index is discontinuous (i.e. $\tilde{z} = 0$) we find

$$R_{\text{left}} = \frac{k_{\tilde{z}} - q_{\tilde{z}}}{k_{\tilde{z}} + q_{\tilde{z}}} \quad \text{and} \quad T_{\text{left}} = \frac{2k_{\tilde{z}}}{k_{\tilde{z}} + q_{\tilde{z}}}. \tag{33}$$

At the second interface, it is convenient to use the coordinate system (x, y_*, z_*) and solve the Maxwell equation

$$\left[\partial_{xx}+\partial_{y_*y_*}+\partial_{z_*z_*}-n^2(z_*)\frac{\partial_{tt}}{c^2}\right]E_{\text{down}}(\mathbf{r},t)=0 \tag{34}$$

with

$$n(z_*)=\begin{cases} n & \text{for } z_*<\dfrac{a}{\sqrt{2}} \\ 1 & \text{for } z_*>\dfrac{a}{\sqrt{2}}. \end{cases} \tag{35}$$

The plane wave solution is

$$\exp[i(k_x x+q_{y_*}y_*-\omega t)] \times\begin{cases} \exp[iq_{z_*}z_*]+R_{\text{down}}\exp[-iq_{z_*}z_*] & \text{for } z_*<\dfrac{a}{\sqrt{2}} \\ T_{\text{down}}\exp[ik_{z_*}z_*] & \text{for } z_*>\dfrac{a}{\sqrt{2}}, \end{cases} \tag{36}$$

where

$$\begin{pmatrix} q_{y_*} \\ q_{z_*} \end{pmatrix}=\mathbf{R}\left(\frac{\pi}{4}\right)\begin{pmatrix} k_{\tilde{y}} \\ q_{\tilde{z}} \end{pmatrix} \tag{37}$$

and

$$\{k_{y_*},k_{z_*}\}=\{q_{y_*},\sqrt{k^2-k_x^2-q_{y_*}^2}\}. \tag{38}$$

As with the first interface, the y_*-component of the wave number is not modified because the discontinuity of the second interface is along the z_*-axis. By matching Eq. (36) at $\tilde{z}=a/\sqrt{2}$, we find

$$R_{\text{down}}=\frac{q_{z_*}-k_{z_*}}{q_{z_*}+k_{z_*}}\exp\left[2iq_{z_*}\frac{a}{\sqrt{2}}\right] \quad \text{and}$$
$$T_{\text{down}}=\frac{2q_{z_*}}{q_{z_*}+k_{z_*}}\exp\left[i(q_{z_*}-k_{z_*})\frac{a}{\sqrt{2}}\right]. \tag{39}$$

We can use the result obtained for the down interface to find the result for the up interface. Making the substitutions $(k_{z_*},q_{z_*})\to-(k_{z_*},q_{z_*})$ and $a/\sqrt{2}\to(a-b)/\sqrt{2}$, we find the reflection and transmission coefficients for the up interface to be

$$R_{\text{up}}=\frac{q_{z_*}-k_{z_*}}{q_{z_*}+k_{z_*}}\exp\left[2iq_{z_*}\frac{b-a}{\sqrt{2}}\right] \quad \text{and}$$
$$T_{\text{up}}=\frac{2q_{z_*}}{q_{z_*}+k_{z_*}}\exp\left[i(q_{z_*}-k_{z_*})\frac{b-a}{\sqrt{2}}\right]. \tag{40}$$

In a similar way, the reflection and transmission coefficients for the right interface can be directly obtained from the coefficients calculated for the left interface. Replacing $k_{\tilde{z}}\leftrightarrow q_{\tilde{z}}$ and observing that the discontinuity is now located at $\tilde{z}=c$, we obtain

$$R_{\text{right}}=\frac{q_{\tilde{z}}-k_{\tilde{z}}}{q_{\tilde{z}}+k_{\tilde{z}}}\exp[2iq_{\tilde{z}}c] \quad \text{and}$$
$$T_{\text{right}}=\frac{2q_{\tilde{z}}}{q_{\tilde{z}}+k_{\tilde{z}}}\exp[i(q_{\tilde{z}}-k_{\tilde{z}})c]. \tag{41}$$

Finally, the outgoing transmission coefficient is given by

$$T_{\text{out}}=T_{\text{left}}R_{\text{down}}R_{\text{up}}T_{\text{right}} =\frac{4k_{\tilde{z}}q_{\tilde{z}}}{(q_{\tilde{z}}+k_{\tilde{z}})^2}\left(\frac{q_{z_*}-k_{z_*}}{q_{z_*}+k_{z_*}}\right)^2 \times\exp\left[iq_{z_*}b\sqrt{2}+i(q_{\tilde{z}}-k_{\tilde{z}})c\right]. \tag{42}$$

The spatial phases of the optical beam in the different regions are then

$$\begin{aligned} &\text{in}: k_x x+k_y y+k_z z=k_x x+k_{\tilde{y}}\tilde{y}+k_{\tilde{z}}\tilde{z}, \\ &\text{left}\to\text{down}: k_x x+k_{\tilde{y}}\tilde{y}+q_{\tilde{z}}\tilde{z}=k_x x+q_{y_*}y_*+q_{z_*}z_*, \\ &\text{down}\to\text{up}: k_x x+q_{y_*}y_*-q_{z_*}z_*, \\ &\text{up}\to\text{right}: k_x x+q_{y_*}y_*+q_{z_*}z_*=k_x x+k_{\tilde{y}}\tilde{y}+q_{\tilde{z}}\tilde{z}, \\ &\text{out}: k_x x+k_{\tilde{y}}\tilde{y}+k_{\tilde{z}}\tilde{z}=k_x x+k_y y+k_z z. \end{aligned} \tag{43}$$

The outgoing beam, which as expected is parallel to the incoming one, is then given by[18,19]

$$E_{\text{out}}(\mathbf{r},t)=E_0\frac{w_0^2}{4\pi}\int dk_x\,dk_y\,\frac{4k_{\tilde{z}}q_{\tilde{z}}}{(q_{\tilde{z}}+k_{\tilde{z}})^2}\left(\frac{q_{z_*}-k_{z_*}}{q_{z_*}+k_{z_*}}\right)^2 \times\exp\left[-\left(k_x^2+k_y^2\right)\frac{w_0^2}{4}\right] \times\exp\left\{i\left[q_{z_*}b\sqrt{2}+(q_{\tilde{z}}-k_{\tilde{z}})c+\mathbf{k}\cdot\mathbf{r}-\omega t\right]\right\}. \tag{44}$$

In the following section, we use the stationary phase method (SPM) to calculate the position of the maximum of the outgoing beam, and consequently the position of the optical beam, at the exit of our dielectric system. The calculation based on the SPM thus represents an alternative method to obtain the optical path. More importantly, the SPM calculation also allows us to obtain the Goos-Hänchen shift.

IV. THE OPTICAL PATH VIA THE STATIONARY PHASE METHOD

The SPM is a basic principle of asymptotic analysis that applies to oscillatory integrals.[22,23] The main idea of the SPM relies on the cancelation of sinusoids with rapidly varying phase, so the dominant contribution to the integral comes when the phase is *stationary*; that is, where the derivative of the phase vanishes. This means that many sinusoids with the same phase can be added together constructively, giving rise to a peaked function. To illustrate this principle let us consider the incoming beam given in Eq. (27). In order to solve the integral we impose that

$$\left[\frac{\partial}{\partial k_x}(\mathbf{k}\cdot\mathbf{r}-\omega t)\right]_{(0,0)}=\left[\frac{\partial}{\partial k_y}(\mathbf{k}\cdot\mathbf{r}-\omega t)\right]_{(0,0)}=0. \tag{45}$$

The subscript (0, 0) tells us that the derivatives have to be calculated at the maximum value of the convolution function, where $k_x=k_y=0$. For the incoming optical beam of Eq. (27), the convolution function is a Gaussian distribution; consequently, the maximum of the incoming beam is located

at $x = y = 0$. This maximum position, which can be obtained without any integration by using Eq. (45), is confirmed by Eq. (1).

A. Partial internal reflection

As discussed in Sec. II, we get partial internal reflection for $\theta < \theta_c$. In this case, the outgoing optical beam has, with respect to the incoming beam, an additional phase given by

$$\phi = q_{z_*} b\sqrt{2} + (q_{\bar{z}} - k_{\bar{z}})c. \tag{46}$$

In order to solve the outgoing integral (44) using the SPM, we must impose the constraints

$$\left[\frac{\partial}{\partial k_x}(\phi + \mathbf{k}\cdot\mathbf{r} - \omega t)\right]_{(0,0)} = \left[\frac{\partial}{\partial k_y}(\phi + \mathbf{k}\cdot\mathbf{r} - \omega t)\right]_{(0,0)} = 0. \tag{47}$$

Observing that

$$\begin{aligned}
\frac{\partial q_{\bar{z}}}{\partial k_{x,y}} &= -\frac{k_{\bar{y}}}{q_{\bar{z}}}\frac{\partial k_{\bar{y}}}{\partial k_{x,y}} = -\frac{k_{\bar{y}}}{q_{\bar{z}}}\left[\cos\theta\frac{\partial k_y}{\partial k_{x,y}} + \sin\theta\frac{\partial k_z}{\partial k_{x,y}}\right],\\
\frac{\partial q_{z_*}}{\partial k_{x,y}} &= \frac{\partial}{\partial k_{x,y}}\left(\frac{q_{\bar{z}} - k_{\bar{y}}}{\sqrt{2}}\right)\\
&= -\frac{k_{\bar{y}} + q_{\bar{z}}}{q_{\bar{z}}\sqrt{2}}\left[\cos\theta\frac{\partial k_y}{\partial k_{x,y}} + \sin\theta\frac{\partial k_z}{\partial k_{x,y}}\right],\\
\frac{\partial k_{\bar{z}}}{\partial k_{x,y}} &= \left[-\sin\theta\frac{\partial k_y}{\partial k_{x,y}} + \cos\theta\frac{\partial k_z}{\partial k_{x,y}}\right],
\end{aligned} \tag{48}$$

we immediately find

$$x = -\left(\frac{\partial\phi}{\partial k_x}\right)_{(0,0)} = 0 \tag{49}$$

and

$$\begin{aligned}
y &= -\left(\frac{\partial\phi}{\partial k_y}\right)_{(0,0)} = b\left(\frac{\sin\theta}{\sqrt{n^2 - \sin^2\theta}} + 1\right)\cos\theta\\
&\quad + c\frac{\sin\theta}{\sqrt{n^2 - \sin^2\theta}}\cos\theta - c\sin\theta\\
&= \left[b + (b + c)\frac{\sin\theta}{\sqrt{n^2 - \sin^2\theta}}\right]\cos\theta - c\sin\theta.
\end{aligned} \tag{50}$$

Thus, we recover Eq. (18) for the shift in the outgoing beam, showing that the SPM represents an alternative way to obtain the geometrical path of optical beams. For partial internal reflection the phase in Eq. (46) is the *only* phase that contributes to the SPM calculation, so this shift in the y-coordinate is the real shift seen in an optical experiment. As we discuss in the next subsection, an *additional* phase appears for total internal reflection (when $\theta > \theta_c$), resulting in an added shift that cannot be predicted by Snell's law.

B. Total internal reflection

As anticipated in the previous section, for $\theta > \theta_c$ an additional phase comes from the double internal reflection coefficient [see Eq. (44)]

$$\left(\frac{q_{z_*} - k_{z_*}}{q_{z_*} + k_{z_*}}\right)^2. \tag{51}$$

Indeed, by observing that

$$\begin{aligned}
k_{z_*}^2 &= \left[1 - \left(\frac{\sin\theta + \sqrt{n^2 - \sin^2\theta}}{\sqrt{2}}\right)^2\right]k^2 + \mathrm{O}\left(k_x^2, k_y\right)\\
&= \left(1 - \frac{n^2}{2} - \sin\theta\sqrt{n^2 - \sin^2\theta}\right)k^2 + \mathrm{O}\left(k_x^2, k_y\right),
\end{aligned} \tag{52}$$

and using Eq. (24), we have $k_{z_*}^2 < 0$. Consequently, Eq. (51) becomes

$$\left(\frac{q_{z_*} - i|k_{z_*}|}{q_{z_*} + i|k_{z_*}|}\right)^2, \tag{53}$$

and we obtain the *additional* phase

$$\varphi = -4\arctan\left(\frac{|k_{z_*}|}{q_{z_*}}\right), \tag{54}$$

which must be included in our calculation. In order to calculate this new contribution, we start from

$$\begin{aligned}
\frac{\partial\varphi}{\partial k_{x,y}} &= -4\frac{q_{z_*}^2}{q_{z_*}^2 + |k_{z_*}|^2}\frac{\partial}{\partial k_{x,y}}\left(\frac{|k_{z_*}|}{q_{z_*}}\right)\\
&= -\frac{4}{q_{z_*}^2 + |k_{z_*}|^2}\left(q_{z_*}\frac{\partial|k_{z_*}|}{\partial k_{x,y}} - |k_{z_*}|\frac{\partial q_{z_*}}{\partial k_{x,y}}\right),
\end{aligned} \tag{55}$$

which, by using the relation

$$q_{z_*}^2 + |k_{z_*}|^2 = (n^2 - 1)k^2 \Rightarrow \frac{\partial|k_{z_*}|}{\partial k_{x,y}} = -\frac{q_{z_*}}{|k_{z_*}|}\frac{\partial q_{z_*}}{\partial k_{x,y}},$$

becomes

$$\frac{\partial\varphi}{\partial k_{x,y}} = \frac{4}{|k_{z_*}|}\frac{\partial q_{z_*}}{\partial k_{x,y}}. \tag{56}$$

Finally, the additional shift in the y-direction, also known as Goos-Hänchen (GH) shift (see Fig. 3), is found to be

$$\begin{aligned}
\delta &= -\left(\frac{\partial\varphi}{\partial k_y}\right)_{(0,0)}\\
&= \frac{4\cos\theta\left(\sin\theta + \sqrt{n^2 - \sin^2\theta}\right)}{k\sqrt{\left(n^2 - 2 + 2\sin\theta\sqrt{n^2 - \sin^2\theta}\right)(n^2 - \sin^2\theta)}}.
\end{aligned} \tag{57}$$

Thus, the SPM allows one to obtain the shift Δy of the outgoing beam both for partial and total internal reflection, with

$$\Delta y = \begin{cases} d & \text{for } \theta < \theta_c \text{ [partial internal reflection]}\\ d + \delta & \text{for } \theta > \theta_c \text{ [total internal reflection]}. \end{cases} \tag{58}$$

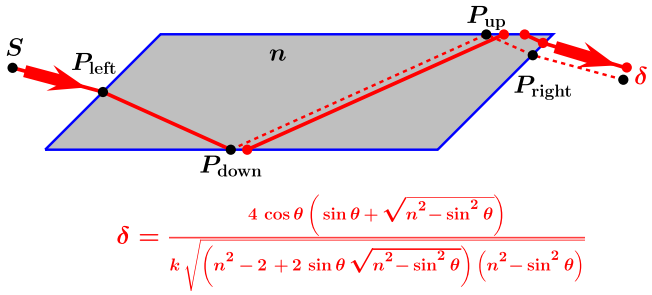

Fig. 3. We illustrate here that, for $\theta > \theta_c$, the geometrical path predicted by Snell's law suffers an additional shift at each internal reflection known as the Goos-Hänchen shift. The net result for our situation is that the outgoing light beam suffers a lateral shift δ, which can be calculated using the stationary phase method (SPM).

In concluding this section, we recall that the GH shift δ cannot be obtained using Snell's law. This additional shift is due to the presence of evanescent waves in the air zones close to the down and up interfaces and cannot be predicted solely from geometry.[32] This phenomenon is similar to the time delay encountered in quantum-mechanical scattering.[33–35]

V. CONCLUSIONS AND OUTLOOK

In this article, we have shown the value of the SPM as a mathematical tool in determining the path of optical beams. Our analysis here, which is carried out for *s*-polarized waves, can be extended to *p*-polarized waves, and gives rise to an outgoing beam transmission coefficient[1,18,19,36]

$$T_{\text{out}}^{(p)} = \frac{4n^2 k_{\bar{z}} q_{\bar{z}}}{(q_{\bar{z}} + n^2 k_{\bar{z}})^2} \left(\frac{q_{z_*} - n^2 k_{z_*}}{q_{z_*} + n^2 k_{z_*}} \right)^2 \times \exp\left[i q_{z_*} b\sqrt{2} + (q_{\bar{z}} - k_{\bar{z}})c \right]. \tag{59}$$

For partial internal reflections, the SPM reproduces the geometrical result predicted by Snell's law: $\Delta y = d$. For total internal reflections, the SPM predicts $\Delta y = d + \delta$, thus accounting for the GH shift. The additional shift δ is proportional to the wavelength of the incoming beam, with a numerical pre-factor of order unity [see Eq. (57)]. The order of magnitude of the GH shift for a double (total) internal reflection is thus relatively small and this makes experimental observations difficult. Note that red lasers ($\lambda \approx 0.633\,\mu$m), whose beam waist is $w_0 = 1$ mm undergo a shift of $\delta \approx 10^{-4} w_0$. Because the shift depends on the number of internal reflections, to make such an experimental measurement possible,[37] we need to amplify the effect by considering, for example, a band of N dielectric blocks. In this case, the final GH shift will be given by $N\delta$.

To guarantee two internal reflections in each block, we impose that the z_*-component at the exit point (P_{right}) be the same as the z_*-component at the entrance point (P_{left}). This condition implies [see Eq. (16)] that $c\tan(\pi/4 - \psi) = b$, which, after simple algebraic manipulations, leads to

$$c = \frac{n^2 + 2\sin\theta\sqrt{n^2 - \sin^2\theta}}{n^2 - 2\sin^2\theta} b. \tag{60}$$

In a forthcoming work, we intend to analytically calculate the integral in Eq. (44) to obtain the outgoing beam profile. This calculation can be carried out by approximating the transmission coefficient in view of the result obtained in Sec. IV.

ACKNOWLEDGMENTS

The authors gratefully thank the referees for their constructive comments and useful suggestions. The authors also thank the Fapesp (SaC) and the CNPq (SdL) for the financial support.

[a]Electronic mail: deleo@ime.unicamp.br

[1]M. Born and E. Wolf, *Principles of Optics* (Cambridge U.P., Cambridge, 1999).
[2]B. E. A. Saleh and M. C. Teich, *Fundamentals of Photonics* (Wiley & Sons, New Jersey, 2007).
[3]M. Kryjevskaia, M. R. Stetzer, and P. R. L. Heron, "Student understanding of wave behavior at a boundary: The relationships among wavelength, propagation speed, and frequency," Am. J. Phys. **80**, 339–347 (2012).
[4]R. Heller, "On the teaching of the Snell-Descartes law of refraction," Am. J. Phys. **16**, 356–357 (1948).
[5]J. W. Shirley, "An early experimental determination of Snell's law," Am. J. Phys. **19**, 507–508 (1951).
[6]C. V. Bertsch and B. A. Greenbaum, "New apparatus for Snell's law," Am. J. Phys. **26**, 340 (1958).
[7]H. E. Bates, "An analogue model for teaching reflection and refraction of waves," Am. J. Phys. **48**, 275–277 (1980).
[8]D. Drosdoff and A. Widom, "Snell's law from an elementary particle viewpoint," Am. J. Phys. **73**, 973–975 (2005).
[9]J. J. Lynch, "Snell's law with large blocks," Phys. Teach. **45**, 180–182 (2007).
[10]L. I. Shiff, *Quantum Mechanics* (McGraw-Hill, New York, 1955).
[11]C. Cohen-Tannoudji, B. Diu, and F. Laloë, *Quantum Mechanics* (Wiley, Paris, 1977).
[12]S. Longhi, "Quantum-optical analogies using photonic structures," Laser Photon Rev. **3**, 243–261 (2009).
[13]X. Chen, X. J. Lu, Y. Ban, and C. F. Li, "Electronic analogy of the Goos-Hänchen effect: A review," J. Opt. **15**, 033001-1–12 (2013).
[14]H. F. Meiners, "Optical analog of quantum-mechanical barrier penetration," Am. J. Phys. **33**, xviii (1965).
[15]P. L. Garrido, S. Goldstein, J. Lukkarinen, and R. Tumulka, "Paradoxical reflection in quantum mechanics," Am. J. Phys. **79**, 1218–1231 (2011).
[16]G. Zhu and C. Singh, "Surveying students understanding of quantum mechanics in one spatial dimension," Am. J. Phys. **80**, 252–259 (2012).
[17]S. De Leo and P. Rotelli, "Localized beams and dielectric barriers," J. Opt. A **10**, 115001-1–5 (2008).
[18]S. De Leo and P. Rotelli, "Laser interacting with a dielectric block," Eur. Phys. J. D **61**, 481–488 (2011).
[19]S. De Leo and P. Rotelli, "Resonant laser tunneling," Eur. Phys. J. D **65**, 563–570 (2011).
[20]M. Selmke and F. Cichos, "Photonic Rutherford scattering: A classical and quantum mechanical analogy in ray and wave optics," Am. J. Phys. **81**, 405–413 (2013).
[21]E. Wigner, "Lower limit for the energy derivative of the scattering phase shift," Phys. Rev. **98**, 145–147 (1955).
[22]R. B. Dingle, *Asymptotic Expansions: Their Derivation and Interpretation* (Academic Press, London 1973).
[23]N. Bleistein and R. Handelsman, *Asymptotic Expansions of Integrals* (Dover, New York, 1975).
[24]D. C. Look, "Novel demonstration of total internal reflection," Am. J. Phys. **49**, 794 (1981).
[25]E. Richard and V. Keuren, "Refractive index measurement using total internal reflection," Am. J. Phys. **73**, 611–615 (2005).
[26]F. Goos and H. Hänchen, "Ein neuer und fundamentaler Versuch zur total-reflexion," Ann. Phys. **436**, 333–346 (1947).
[27]S. R. Seshadri, "Goos-Hänchen beam shift at total internal reflection," J. Opt. Soc. Am. A **5**, 583–585 (1988).

[28]A. Aiello, "Goos-Hänchen and Imbert-Federov shifts: A novel perspective," New J. Phys. **14**, 013058-1–12 (2012).
[29]K. Y. Bliokh and A. Aiello, "Goos-Hänchen and Imbert-Fedorov beam shifts: An overview," J. Opt. **15**, 014001-1–16 (2013).
[30]M. Andrews, "The evolution of free wave packets," Am. J. Phys. **76**, 1102–1107 (2008).
[31]F. Mooney, "Snell's law equivalent to the conservation of tangential momentum," Am. J. Phys. **19**, 385 (1951).
[32]F. P. Zanella, D. V. Magalhes, M. M. Oliveira, R. F. Bianchi, and L. Misoguti, "Frustrated total internal reflection: A simple application and demonstration," Am. J. Phys. **71**, 494–496 (2003).
[33]K. Yasumoto and Y. Oishi, "A new evaluation of the Goos-Hänchen shift and associated time delay," J. Appl. Phys. **54**, 2170–2176 (1983).
[34]W. van Dijk and K. A. Kiers, "Time delay in simple one dimensional systems," Am. J. Phys. **60**, 520–527 (1992).
[35]L. de la Torre, "Wave packet distortion and time delay," Am. J. Phys. **65**, 123–125 (1997).
[36]C. Bahrim and W. T. Hsu, "Precise measurements of the refractive indices for dielectrics using an improved Brewster angle method," Am. J. Phys. **77**, 337–344 (2009).
[37]N. J. Harrick, "Study of physics and chemistry of surfaces from frustrated total internal reflections," Phys. Rev. Lett. **4**, 224–226 (1960).

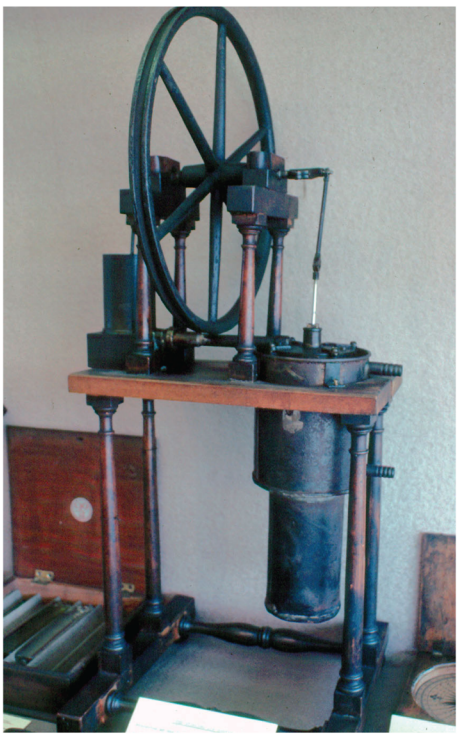

Stirling Engine

I photographed this Stirling Engine in the summer of 1978 on a visit to the physics department at Glasgow University. It was one of many scientific items on display in the cabinets lining the faculty and staff lunch room. Robert Stirling (1790-1876) was a Scottish clergyman and inventor who patented the device in 1816, and put it to practical use two years later for pumping water from a quarry. (Notes and photograph by Thomas B. Greenslade, Jr., Kenyon College)